Magnetic properties of chiral magnets with impurities

A. M. Belemuk *
Institute for High Pressure Physics, Russian Academy of Science, Troitsk 108840, Russia

S. M. Stishov
P. N. Lebedev Physical Institute, Russian Academy of Sciences, Moscow 119991, Russia

(Received 1 February 2023; revised 5 April 2023; accepted 24 April 2023; published 5 May 2023)

In the framework of the spin-lattice model we investigate a role of impurity doping on the evolution of the magnetic susceptibility and the development of the magnetic moment in magnetic field in chiral magnets. We focus on a particular class of silicide—Fe- and Co-doped MnSi. We introduce two feasible models accounting for different possible impurity arrangements in a real compound. Our calculations are based on the Monte Carlo method for classical spins. We are interested in the magnetic response and the degradation of the magnetic phase transition upon doping. We compare the calculated susceptibility with available experimental data in these compounds. We illustrate features of the behavior of the magnetic susceptibility by the corresponding spin patterns showing the deterioration of the spiral structure with temperature and the corresponding formation of ring-shape patterns in Bragg intensity profiles.

DOI: 10.1103/PhysRevB.107.184411

I. INTRODUCTION

Chiral helimagnets have a wealth of intriguing properties involving itinerant magnetism [1], anomalous behavior of thermodynamic quantities [2,3], quantum phase transitions [4–6], and transport properties [7,8]. Particularly interesting is the investigation of the helimagnets under compositional tuning in transition-metal compounds such as $Mn_{1-x}Fe_xSi$ and $Mn_{1-x}Co_xSi$ [9–11]. Increasing impurity concentration mimics the properties of a helimagnet under pressure and enables one to get insight into the nature of the quantum fluctuations and magnetic phase diagram at high pressure.

At low temperature these compounds exhibit long-wavelength helimagnetic modulation with a sharp signature of the first order transition which degrades with applying the magnetic field, or increasing the concentration of impurities [9,10]. Thermodynamic measurements indicate a puzzling universal line for the difference between heat capacity at zero magnetic field and heat capacity at $B = 9$ T as a function of temperature [12]. This line exposes an independence of the fluctuation contribution to the heat capacity on impurity concentration [12].

Evolution of the helimagnetic fluctuations with doping originates presumably from the existence of exotic magnetic structures and the interplay of localized and itinerant magnetism. Experiments in $Mn_{1-x}Fe_xSi$ and $Mn_{1-x}Co_xSi$ show [13,14] that with increasing doping (i) the transition temperature decreases monotonously and vanishes at $x_c \sim 0.17$; (ii) the helimagnetic Bragg peaks (with long-range order) disappear at a lower concentration $x^* \sim 0.11$; (iii) in the range $x^* < x < x_c$ the helimagnetic correlations are of short-range order; and (iv) there exists the precursor phase at temperature slightly above of T_c, signaling that the chiral fraction of the magnetic correlations sets in even in $x^* < x < x_c$.

In the present study we are interested in the behavior of the magnetic susceptibility and the induced magnetic moment in a helimagnet with impurities. Our consideration is based on the assumption that magnetic properties of the system can be well modeled by a picture of localized spins in the framework of the lattice spin Hamiltonian. Our goal is to find out how many results consistent with experiment can be deduced from this simple base assumption. In our previous study [15] we investigated the dependence of the specific heat on the impurity concentration. We demonstrated that the model of localized spins correctly reproduces the evolution of the specific heat and the degradation of the first-order magnetic transition with increasing impurity concentration.

The behavior of the magnetic susceptibility found in the present work shows similar degradation of the magnetic phase transition. However, the description of magnetic properties is more subtle as it involves the itinerant nature of the magnetic moment in these compounds. The experiment shows a considerable change of the value of the atomic magnetic moment upon doping; the effective magnetic moment decreases from $\mu_{\text{eff}} = 2.2\mu_B$ f.u.$^{-1}$ at $x = 0$ to $\mu_{\text{eff}} = 1.3\mu_B$ f.u.$^{-1}$ at $x = 0.2$ [11]. To be able to account for these changes we extend the model of localized spins to include the effective magnetic moment $\mu(x)$ depending on the impurity concentration.

This paper is organized as follows. In Sec. II we introduce the model Hamiltonian that incorporates impurity spins as localized spins coupled with the regular ones by modified exchange and Dzyaloshinskii-Moriya coupling constants. We introduce two feasible models for arrangement of impurities and their coupling with surroundings. In these models an inherent itinerant nature of magnetic moment in doped

*abel@hppi.troitsk.ru

compounds is ignored; the evolution of magnetic properties originates solely from distorting the spin structure with doping. In Sec. III we present the corresponding results.

The model of localized spins predicts that the position of the susceptibility peak is shifted to lower temperature with increasing the concentration x. The induced magnetic moment increases with magnetic field B with a rate depending on x. We calculate an average spin configuration $\langle \mathbf{S_r} \rangle$, which enables us to illustrate changes taking place in the system with doping. We find that the peak of the magnetic susceptibility seen at zero and finite values of B correlates with the transition from a one-spiral state to a multispiral structure with increasing temperature as is revealed by Bragg intensity profiles. To be able to compare with experiment we have to account for the real change of the magnitude of the atomic magnetic moment upon doping. We phenomenologically add impurity-dependent magnetic moment for localized spins. This is analyzed in Sec. IV.

II. MODEL

We use a standard lattice spin model [16–18] involving the ferromagnetic exchange and Dzyaloshinskii-Moriya (DM) spin-spin interactions

$$H = -\sum_{\boldsymbol{r},\boldsymbol{r}'} [J_{\boldsymbol{r}\boldsymbol{r}'} \boldsymbol{S_r} \cdot \boldsymbol{S_{r'}} + D_{\boldsymbol{r}\boldsymbol{r}'} (\boldsymbol{S_r} \times \boldsymbol{S_{r'}}) \cdot \boldsymbol{n_{rr'}}] - B \sum_{\boldsymbol{r}} S^z_{\boldsymbol{r}}. \tag{1}$$

Variables $\mathbf{S_r} = (S^x_{\mathbf{r}}, S^y_{\mathbf{r}}, S^z_{\mathbf{r}})$ are treated as classical spins of unit length. Amplitudes of the exchange and DM interaction are supposed to be nonzero only for the nearest neighbors, $J_{\boldsymbol{r}\boldsymbol{r}'} = J$ and $D_{\boldsymbol{r}\boldsymbol{r}'} = D$. A unit vector $\boldsymbol{n_{rr'}}$ is directed from $\boldsymbol{r}$ to $\boldsymbol{r}'$, $\boldsymbol{r}'$ indexes a half of the nearest neighbors of $\mathbf{r}$, $\mathbf{r}' = \mathbf{r} + \hat{\mathbf{x}}, \mathbf{r} + \hat{\mathbf{y}}, \mathbf{r} + \hat{\mathbf{z}}$, and the lattice spacing is taken to be unity, $a = 1$. The third term is the Zeeman term; an external magnetic field B is applied in the z direction.

We consider two models for an arrangement of doped impurities. In the first model (model A) we assume that upon doping a regular spin $\boldsymbol{S_r}$ is replaced by an effective impurity spin $\boldsymbol{S^c_r}$, which is similar to the regular one. The impurity spins are coupled with neighboring regular spins by some modified exchange and DM coupling constants $J_{\boldsymbol{r}\boldsymbol{r}'} = J'$ and $D_{\boldsymbol{r}\boldsymbol{r}'} = D'$. If two impurity spins happen to occur in neighboring sites the corresponding coupling constant is forced to be zero. As a result the effective Hamiltonian for a compound with impurities is formally described by Eq. (1) with randomly chosen sites for positions of the impurities and correspondingly modified coupling constants $J_{\boldsymbol{r}\boldsymbol{r}'}$ and $D_{\boldsymbol{r}\boldsymbol{r}'}$.

In the second model (model B) impurity spins $\boldsymbol{S^c_i}$ are placed at interstitial positions of the original lattice and we additionally assume that there is no dynamics for these spins, i.e., they are considered effectively frozen. These interstitial spins are coupled with their eight nearest neighbors by exchange interaction

$$H_{\text{imp}} = -\sum_{i,\boldsymbol{r}(i)} J^c_{i\boldsymbol{r}} \boldsymbol{S^c_i} \cdot \boldsymbol{S_r} \tag{2}$$

with some random coupling amplitude $J^c_{i\boldsymbol{r}}$ uniformly distributed over interval [0,1].

Models A and B ignore the difference in magnetic moments of impurity and regular atoms, which is essential in compounds such as $Mn_{1-x}Fe_xSi$ and $Mn_{1-x}Co_xSi$. Their predictions therefore have a limited range of applicability. The end compounds FeSi and CoSi are not magnetic and cannot be modeled by a picture of localized spins. We consider doping levels less than $x = 0.25$. Nevertheless, models A and B are interesting by their own as they describe transformations in spin structures taking place totally due to disorder effects in exchange and DM coupling constants.

The Monte Carlo (MC) simulation was carried out using a standard single-site Metropolis algorithm on a $L \times L \times L$ lattice of size $L = 30$ with periodic boundary conditions. In the calculation we fix the parameter $J = 1$ which serves as a unit of temperature. We made 10^6 MC steps per spin (MCS) to equilibrate the system and next 10^6 MCS (and up to 10^7 MCS in separate runs) to gain statistics. Results are also averaged over different impurity distributions; typically we consider $n_i = 8$ impurity distributions.

From the simulation we directly find the dependence of the induced magnetization $M_z = \langle m_z \rangle$, $\langle m_z \rangle = 1/N \sum_{\mathbf{r}} \langle S^z_{\boldsymbol{r}} \rangle$, $N = L^3$, on the magnetic field. For the model A this average includes all spins of the lattice, both the regular and the impurity ones. For the model B only regular spins are taken into account. We find the magnetic susceptibility from the corresponding variance, $\chi = N(\langle m_z^2 \rangle - \langle m_z \rangle^2)/T$.

Analyzing spin configurations $\langle \mathbf{S_r} \rangle$, we find the corresponding Bragg intensity profiles, $I(\mathbf{q}) \propto |\langle \mathbf{S_q} \rangle|^2$, $\langle \mathbf{S_q} \rangle = 1/N \sum_{\mathbf{r}} \langle \mathbf{S_r} \rangle e^{-i\mathbf{q}\cdot\mathbf{r}}$. A spin spiral with a wave vector $\mathbf{k}$, $\mathbf{S_r} = S_\perp[\mathbf{e}_1 \cos(\mathbf{k}\cdot\mathbf{r}) + \mathbf{e}_2 \sin(\mathbf{k}\cdot\mathbf{r})]$, is characterized by two separate peaks of the $I(\mathbf{q})$ at points $\boldsymbol{q} = \pm\mathbf{k}$. This and other spin structures are convenient to analyze with the help of a projected intensity, $I^*(\bar{\mathbf{q}}) = \sum_{q_z(q_y)} I(q_x, q_y, q_z)$, which shows the profile of $I(\mathbf{q})$ projected onto (q_x, q_y) or, respectively, onto the (q_x, q_z) plane. For a spin spiral the projected intensity is $I^*(\bar{\mathbf{q}}) = (S^2_\perp/2)(\delta_{\bar{\mathbf{q}},\bar{\mathbf{k}}} + \delta_{\bar{\mathbf{q}},-\bar{\mathbf{k}}})$, where two-dimensional vectors $\bar{\mathbf{q}}, \bar{\mathbf{k}}$ are projections of vectors $\mathbf{q}, \mathbf{k}$ onto the corresponding plane. In a magnetic field there appears an additional peak at $\bar{\boldsymbol{q}} = 0$ corresponding to a conical state, $I^*(\bar{\mathbf{q}}) = S^2_\parallel \delta_{\bar{\boldsymbol{q}},0} + (S^2_\perp/2)(\delta_{\bar{\mathbf{q}},\bar{\mathbf{k}}} + \delta_{\bar{\mathbf{q}},-\bar{\mathbf{k}}})$. Presenting $I(\boldsymbol{q})$ we set $2\pi/L$ as a unit length in the $\mathbf{q}$ space.

III. RESULTS AND DISCUSSION

To illustrate our results we set coupling constants for regular spins $J = 1.0$ and $D = 0.75$. This leads to a pitch length of a spin spiral equal to $\ell \approx 10a$. A similar magnetic behavior occurs if the magnitude of the DM coupling parameter lies in the interval $0.4 < D < 2$ [19,20]. For the coupling parameters of the regular and impurity spins we adopt $J' = 0.1$ and $D' = 0$. This is consistent with the experimental findings that indicate that impurities substantially suppress the helimagnetic order. More details on the choice of the coupling parameters of the effective model are given in Ref. [15].

Figure 1 shows the evolution of the temperature dependence of the magnetic susceptibility χ with increasing impurity concentration x. Results are shown in zero applied magnetic field. We assume that the dopant concentration x in $Mn_{1-x}Fe/Co_xSi$ is related to the fraction of impurity spins in

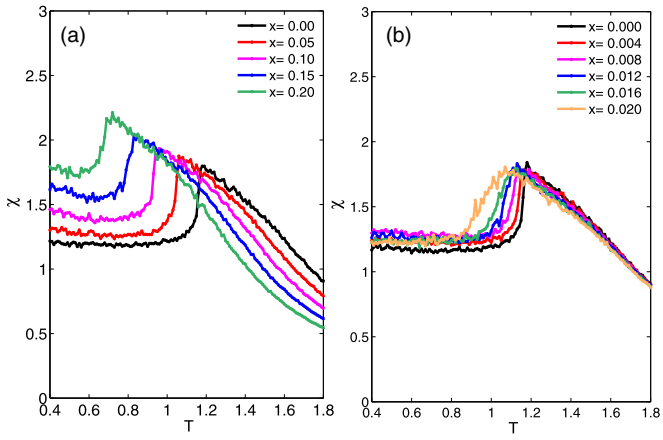

FIG. 1. Susceptibility as a function of temperature for different values of doping concentration x for models A (a) and B (b).

model A. In model B parameter x corresponds to a fraction of interstitial spins in the original regular lattice.

Both evolution dependencies have similar features. In particular, the low-temperature part is characterized by a shoulder; the shoulder is wider for a lower impurity concentration. There is a steplike peak at the temperature of the magnetic phase transition, and then a further decrease of χ with increasing temperature. Model A demonstrates a substantial dependence of the peak position on the impurity concentration; the peak shifts to lower temperature with increasing x. For model B this shift is much less pronounced. The shift of the peak is consistent with experimental findings (compare, e.g., Fig. 14 in Ref. [10] and Fig. 1 in Ref. [11]). At the same time there is a distinction; the experiment indicates the lowering of the peak with increasing x while our results demonstrate that the amplitude of the maximum gets a little bit higher with increasing doping concentrations. We relate this discrepancy with our model assumption that a doped impurity spin possesses the same local magnetic moment as a regular one. In reality such an assumption is a rather rude approximation. In Sec. IV we take into account the doping dependence of the local magnetic moment. This will result in lowering the peak of χ with doping. The observed increase of χ in Fig. 1 comes from a factor $1/T$ in the definition of susceptibility via spin fluctuations, $\chi \sim \langle(\Delta m_z)^2\rangle/T$.

To get insight into the behavior of the magnetic susceptibility shown in Fig. 1 and understand the nature of the susceptibility peak, we illustrate in Figs. 2 and 3 changes happening in the spin system of models A and B with increasing temperature. In Fig. 2 we show the results for model A; the upper pattern is taken at temperature $T = 0.70$ which is lower than T_c, and the bottom one at temperature $T = 0.90$ which is a little bit higher than T_c. At a lower temperature one observes well-defined peaks of the projected Bragg intensity $I^*(\bar{\boldsymbol{q}})$ coming from a formation of the spiral structure, which appears as two separate peaks of I^*. At a higher temperature one sees the formation of a pattern with ring-shape structure of the Bragg intensity characteristic of helimagnets. Such patterns are widely seen just above the T_c in numerous neutron experiments [13,21–23].

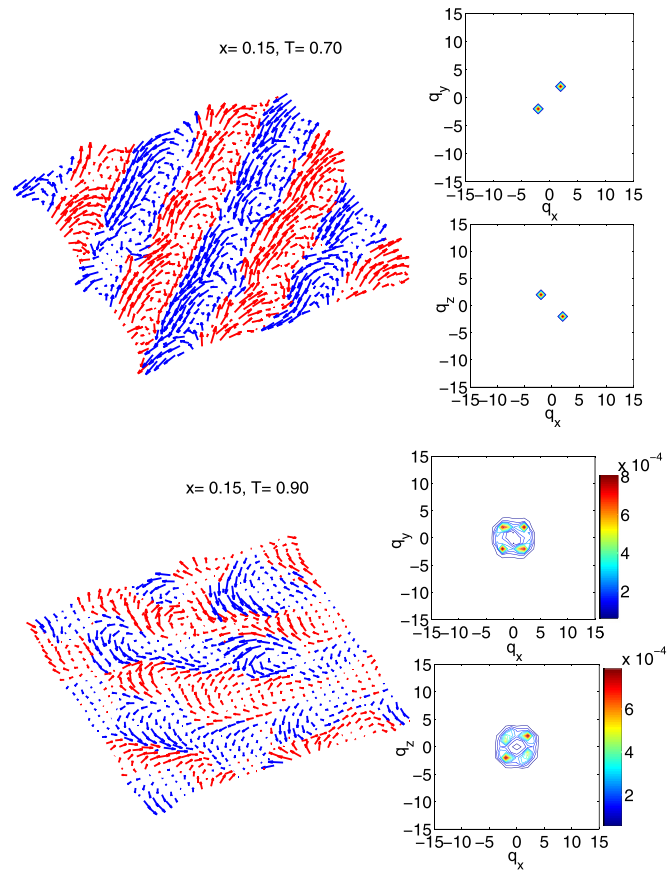

FIG. 2. Spin configuration and profile of the projected Bragg intensity for model A; doping concentration $x = 0.15$.

In Fig. 3 we show spin configurations for model B. We want to illustrate changes in the spin configuration happening at the left slope of the susceptibility peak presented in Fig. 1. The lower temperature $T = 1.00$ corresponds to the base of the slope and the higher $T = 1.10$ to the crest of χ. One sees that the transition at T_c goes through the distortion of the spiral spin structure. First magnetic vortices start penetrating into the spiral pattern. This leads to a change of the form of the Bragg spots; they becomes elongated quasipoints in $\boldsymbol{q}$ space. Then with increasing temperature the structure of Bragg spots is further distorted; elongated spots steadily transform into a quasiwhirl structure that finally comes to a ring-shape structure of the projected Bragg intensity $I^*(\bar{\boldsymbol{q}})$.

Another interesting feature seen in the behavior of a neutron scattering function is the dependence of the pitch of helical modulation ℓ on impurity concentration; ℓ decreases monotonously from 18.2 nm for $x = 0$ to 6.2 nm for $x = 0.14$ [13]. Concurrently, the well-defined Bragg peaks smear and completely disappear for $x > x^* = 0.11$. Broad isotropic rings of scattering intensity arise at $x > x^* = 0.11$ which persist down to the lowest temperature measured (see Figs. 1 and 2 of Ref. [13]). Our results for models A and B do not demonstrate such smearing with increasing the doping level x. We relate it with inadequacy of the model of localized spins to capture the real physics happening in the magnetic state upon doping at $x > 0.11$. The picture of localized spins has some resemblance to experiment for impurity concentrations lower than

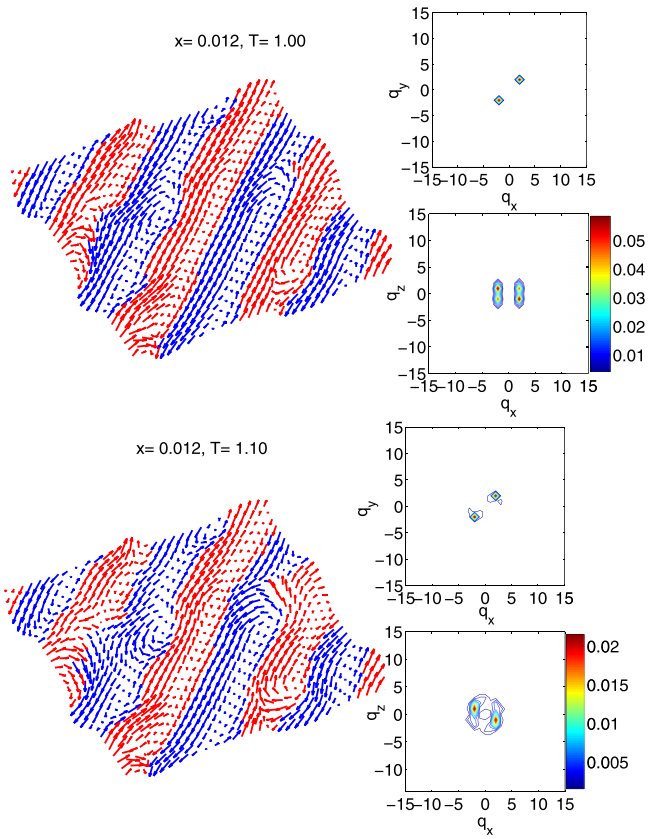

FIG. 3. Spin configuration and profile of the projected Bragg intensity for model B; doping concentration $x = 0.012$.

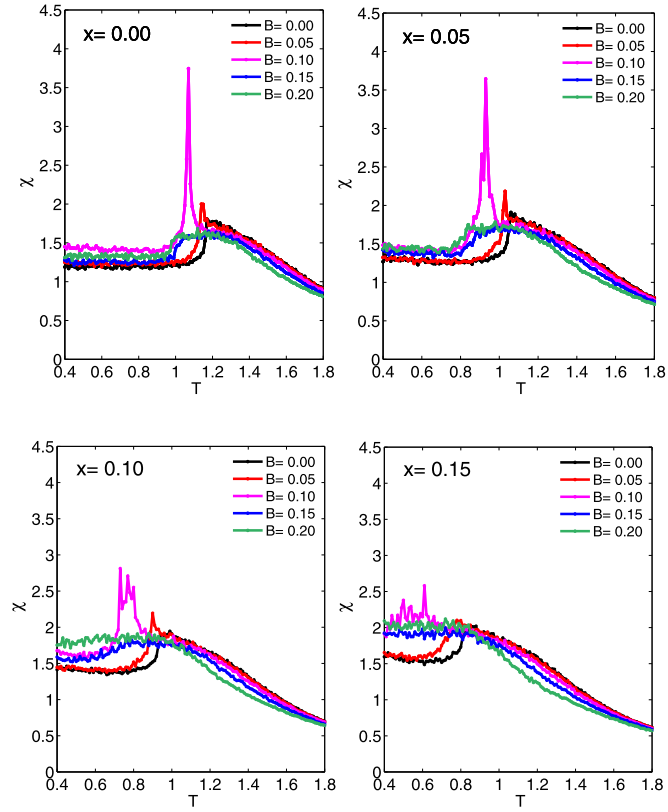

FIG. 4. Susceptibility as a function of temperature for different values of magnetic field B and doping concentration x for model A.

$x \approx 0.10$. In this range it correctly predicts the smearing and transformation of Bragg spots with temperature.

Next, we analyze the behavior of the magnetic susceptibility in a finite applied magnetic field. In Fig. 4 we illustrate the evolution of the susceptibility for model A calculated for various impurity concentrations x. Apart from a shoulder and a steplike peak seen at $B = 0$, the features discussed earlier, there appears another sharp peak superimposed on the first broad one. This second sharp peak is seen at $B = 0.05$ and $B = 0.1$; it moves towards lower temperature with increasing x. With increasing field it merges with the first peak and transforms into a broad hump similar to the hump seen in specific heat measurements [3,10,24]. The sharp peak observed at $B = 0.1$ becomes wider with increasing x and gradually transforms into a shoulder at $x = 0.15$ characterized by enhanced fluctuations of χ due to the occurrence of various metastable topological textures and mesophases [25].

The sharp peak signalizes a transition between spin patterns of different spiral multiplicity. This is clearly seen from an inspection of the corresponding Bragg intensity profiles. In Fig. 5 we show $I^*(\bar{\boldsymbol{q}})$ at field $B = 0.1$ projected onto a plane (q_x, q_z) for selected temperatures in the vicinity of the sharp peak. At $x = 0.05$ the sharp peak of χ is associated with a transition from a single spiral spin state with two main peaks of $I^*(\bar{\boldsymbol{q}})$ (a slight spot at $\boldsymbol{q} = 0$ characteristic of conical magnetic structure is always present in nonzero magnetic field), to one central peak at $\boldsymbol{q} = 0$. With increasing x, at $x = 0.10$, the transition goes from a one-spiral state to a multispiral state; at least three main peaks are seen in $I^*(\bar{\boldsymbol{q}})$ at $T = 0.8$. At even higher concentration, $x = 0.15$, the transition is more complicated. Here the multispiral state persists in a finite temperature range due to proliferation of long-living metastable vortexlike spin patterns. The transition goes into another multispiral state that is characterized by a $I^*(\bar{\boldsymbol{q}})$ profile with five main peaks.

Next, we consider the dependence of the induced magnetic moment in an applied magnetic field. We illustrate our results for temperature $T = 0.5$ at which spins would be arranged into a spiral in zero applied field. The dependencies of magnetization M_z for different x are given in Fig. 6. The dependence

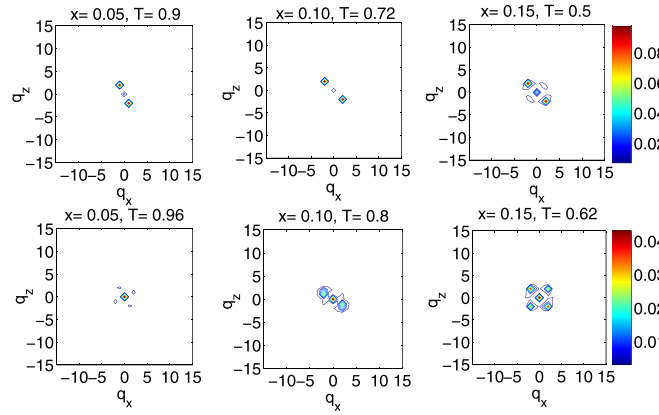

FIG. 5. Profiles of the projected Bragg intensity for model A in the applied field $B = 0.1$.

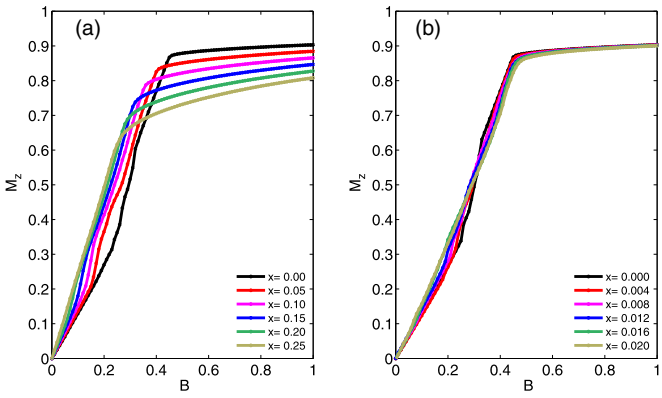

FIG. 6. Magnetic moment as a function of applied magnetic field for different values of doping concentration x for models A (a) and B (b).

$M_z(B)$ demonstrates two regimes: the initial growth at $B \lesssim 0.4$ and the subsequent quasishoulder at which the magnetic moment shows the tendency to a saturation. For model A the value of saturation is lower for higher x while for model B the dependence of $M_z(B)$ on the doping is less pronounced and shows no sign of dependence of the quasishoulder on x. For model A there are some irregular jumps in the magnetization dependence originating from metastable spin structures formed in a magnetic field. The magnitude of magnetization at the quasishoulder is lower for a specimen with higher x, which can be explained as higher dopant concentration increases the disorder in the system. Significant temperature fluctuations take place as well, leading to notable difference of the magnetization at the quasishoulder from the saturation value ($M_z = 1$). Experiments demonstrate behavior similar to our results for model A, although with quite different value of the saturation magnetization [9,11,26]. The value of the saturation magnetization should also account for the change of the local magnetic moment upon doping. We return to this question in Sec. IV.

With increasing the applied magnetic field the polarization of the system along z should proceed. In Fig. 7 we illustrate spin patterns for model B (for model A spin patterns are very similar). With increasing magnetic field the polarization of the system takes place concurrently with the formation of whirls. At a lower field $B = 0.15$ the spirals significantly distort due to initializing whirls. At higher field $B = 0.30$ a part of the system is almost polarized in the z direction while the rest of the system is taken by vortices. At higher field all vortices are melted and the system becomes fully polarized in the z direction. The nonzero value of $\langle S^z \rangle$ shows itself as a separate Bragg spot at $q_z = 0$, which is seen in Fig. 7.

From two analyzed models it seems that only model A is relevant for experimental situation for impurity concentrations lower than $x \approx 0.1$. In the next section we extend model A to account for a change of a local magnetic moment with doping. Model B shows properties that are far from experimental results in doped MnSi. We think that experimental realization of model B could be feasible in systems with frozen disorder. A spin-glass ground state is possibly realized in $Mn_{1-x}Co_xSi$ at high doping level [27] although far beyond the scope of model B.

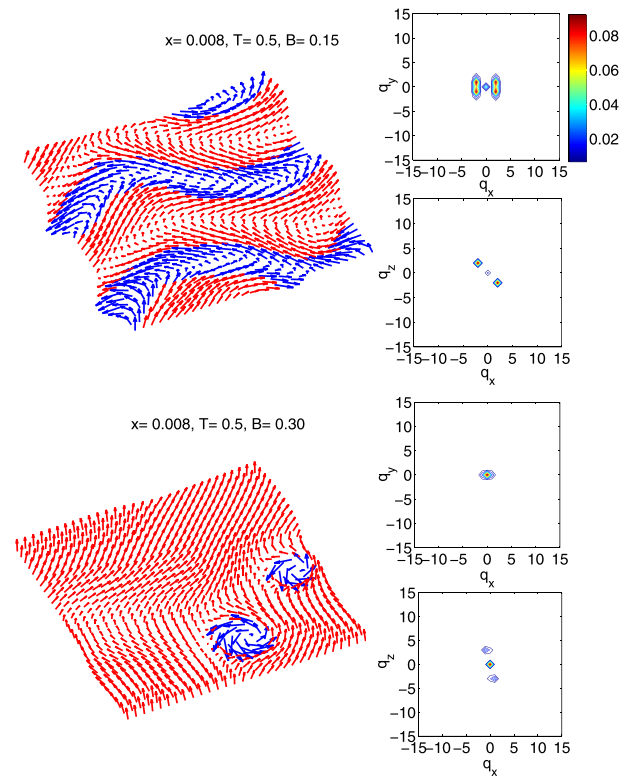

FIG. 7. Spin configuration and profile of the projected Bragg intensity for model B in applied fields $B = 0.15$ and $B = 0.30$.

IV. EXTENDED MODEL

The main drawback of the considered models is that they ignore a change of the local magnetic moment upon a substitution of Fe or Co for a regular atom Mn. Experimental data unambiguously show [10,11] that the atomic magnetic moment substantially changes upon doping. Estimates based on the Curie-Weiss constant give the effective magnetic moment $\mu_{\text{eff}} = 2.2\mu_B$ f.u.$^{-1}$ for $x = 0$ and it diminishes up to $\mu_{\text{eff}} = 1.3\mu_B$ f.u.$^{-1}$ for $x = 0.2$ [11]. This change of the local magnetic moment does not enter model Hamiltonian, Eq. (1). To fix this shortcoming we extend model A and phenomenologically include doping dependence into an atom magnetic moment $\mu(x)$. We treat parameter μ as a ratio of μ_{eff} to $\mu_{\text{eff}}(x = 0)$, where μ_{eff} is taken from the experimental data of Ref. [11]. The resulting values of μ are given in Table I. The extended Hamiltonian reads

$$H = -\sum_{\boldsymbol{r},\boldsymbol{r}'} [J_{\boldsymbol{r}\boldsymbol{r}'}\boldsymbol{S}_{\boldsymbol{r}} \cdot \boldsymbol{S}_{\boldsymbol{r}'} + D_{\boldsymbol{r}\boldsymbol{r}'}(\boldsymbol{S}_{\boldsymbol{r}} \times \boldsymbol{S}_{\boldsymbol{r}'}) \cdot \boldsymbol{n}_{\boldsymbol{r}\boldsymbol{r}'}] - B\mu \sum_{\boldsymbol{r}} S^z_{\boldsymbol{r}}. \tag{3}$$

TABLE I. Parameters of the extended model. x is the doping, μ_{eff} is the effective atom magnetic moment (in μ_B f.u.$^{-1}$) according to Ref. [11], and μ is the parameter of the extended model, Eq. (3).

x	0.0	0.05	0.10	0.15	0.20	0.25
μ_{eff}	2.2	1.97	1.6	1.3	1.3	1.3
μ	1.0	0.89	0.7	0.6	0.6	0.6

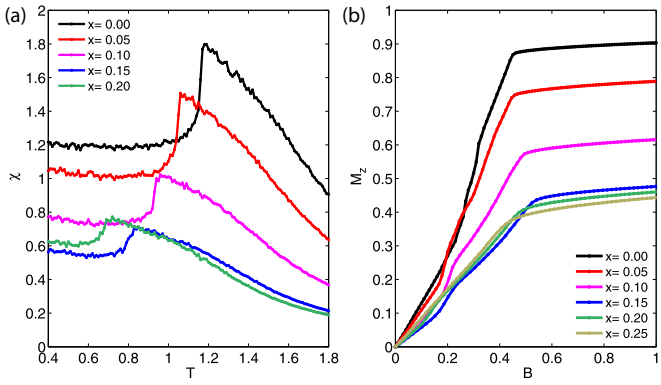

FIG. 8. Dependencies of susceptibility on temperature (a) and induced magnetic moment on magnetic field (b) for different values of doping x for the extended model, Eq. (3).

The evolution of the magnetization $M_z = \langle \mu/N \sum_{\boldsymbol{r}} S^z_{\boldsymbol{r}} \rangle$ and the susceptibility $\chi = \langle (\Delta M_z)^2 \rangle / NT$ with increasing doping concentration x is due to two effects. The first, doping Fe makes neighboring Mn atoms lose their ordering due to perturbed couplings $J_{\boldsymbol{r}\boldsymbol{r}'}$ and $D_{\boldsymbol{r}\boldsymbol{r}'}$. This effect was analyzed in the framework of model A. The second, explicit dependence of μ on x comes from an itinerant nature of electron magnetism in doped $Mn_{1-x}Fe/Co_xSi$.

The temperature dependence of χ as well as a field dependence of M_z is provided in Fig. 8. With increasing x, one sees a gradual diminishing of the peak in χ and its shift to lower temperatures that conform with experiment, as presented, e.g., in Fig. 1 of Ref. [11] and Fig. 14 of Ref. [10]. The doping dependence of μ substantially changes the behavior of the induced magnetization as well; the saturation value of M_z follows a notable decrease with x in accordance with experiment [11,26]. This implies that doping involves significant changes in the magnetic state of the system and the dependence of μ on x should be considered for a successful description of the magnetic properties of the $Mn_{1-x}Fe/Co_xSi$ family.

V. CONCLUSION

In summary, we considered a magnetic response of a helimagnet with impurities on an applied magnetic field. We modeled the magnetic behavior in terms of localized classical spins on a lattice and introduced two feasible models of arrangements of impurities. The first of two models, model A, captures some of the main experimental features observed in helimagnets. In particular, it predicts the impurity-dependent peak of the susceptibility which is accompanied by a formation of vortexlike structures in a helimagnet. The calculated dependence of the susceptibility on impurity concentration supports the view that there is a cloud of helical fluctuations spreading over a significant range of concentrations and temperatures in doped compounds [12].

At the same time the presented models of localized spins are incapable of describing the evolution of the Bragg intensity profiles and the corresponding spin patterns with doping levels greater than $x = 0.10$ at low temperature. The classical models of localized spins do not allow one to infer definite conclusions about the presence or absence of a quantum critical point in MnSi, and what is the nature of the true ground state of an itinerant helimagnet with impurities.

[1] M. Brando, D. Belitz, F. M. Grosche, and T. R. Kirkpatrick, Rev. Mod. Phys. **88**, 025006 (2016).

[2] A. E. Petrova and S. M. Stishov, J. Phys.: Condens. Matter **21**, 196001 (2009).

[3] S. M. Stishov and A. E. Petrova, Phys. Usp. **54**, 1117 (2011).

[4] S. M. Stishov, Phys. Usp. **59**, 866 (2016).

[5] S. M. Stishov and A. E. Petrova, Phys. Usp. **60**, 1268 (2017).

[6] C. Pfleiderer, A. Neubauer, S. Mühlbauer, F. Jonietz, M. Janoschek, S. Legl, R. Ritz, W. Münzer, C. Franz, P. G. Niklowitz, T. Keller, R. Georgii, P. Böni, B. Binz, A. Rosch, U. K. Rößler, and A. N. Bogdanov, J. Phys.: Condens. Matter **21**, 164215 (2009).

[7] M. Lee, W. Kang, Y. Onose, Y. Tokura, and N. P. Ong, Phys. Rev. Lett. **102**, 186601 (2009).

[8] A. Neubauer, C. Pfleiderer, B. Binz, A. Rosch, R. Ritz, P. G. Niklowitz, and P. Böni, Phys. Rev. Lett. **102**, 186602 (2009).

[9] A. E. Petrova, S. Y. Gavrilkin, G. V. Rybalchenko, D. Menzel, I. P. Zibrov, and S. M. Stishov, Phys. Rev. B **103**, L180401 (2021).

[10] A. Bauer, A. Neubauer, C. Franz, W. Münzer, M. Garst, and C. Pfleiderer, Phys. Rev. B **82**, 064404 (2010).

[11] L. J. Bannenberg, F. Weber, A. J. E. Lefering, T. Wolf, and C. Pappas, Phys. Rev. B **98**, 184430 (2018).

[12] A. E. Petrova, A. M. Belemuk, and S. M. Stishov, arXiv:2209.08368.

[13] L. J. Bannenberg, R. M. Dalgliesh, T. Wolf, F. Weber, and C. Pappas, Phys. Rev. B **98**, 184431 (2018).

[14] C. Pappas, A. O. Leonov, L. J. Bannenberg, P. Fouquet, T. Wolf, and F. Weber, Phys. Rev. Res. **3**, 013019 (2021).

[15] A. M. Belemuk and S. M. Stishov, Phys. Rev. B **104**, 064404 (2021).

[16] S. D. Yi, S. Onoda, N. Nagaosa, and J. H. Han, Phys. Rev. B **80**, 054416 (2009).

[17] A. Hamann, D. Lamago, T. Wolf, H. v. Löhneysen, and D. Reznik, Phys. Rev. Lett. **107**, 037207 (2011).

[18] S. Buhrandt and L. Fritz, Phys. Rev. B **88**, 195137 (2013).

[19] A. M. Belemuk and S. M. Stishov, Phys. Rev. B **95**, 224433 (2017).

[20] A. M. Belemuk and S. M. Stishov, Phys. Rev. B **101**, 144426 (2020).

[21] S. V. Grigoriev, S. V. Maleyev, A. I. Okorokov, Yu. O. Chetverikov, R. Georgii, P. Böni, D. Lamago, H. Eckerlebe, and K. Pranzas, Phys. Rev. B **72**, 134420 (2005).

[22] S. V. Grigoriev, S. V. Maleyev, E. V. Moskvin, V. A. Dyadkin, P. Fouquet, and H. Eckerlebe, Phys. Rev. B **81**, 144413 (2010).

[23] C. Pappas, E. Lelièvre-Berna, P. Falus, P. M. Bentley, E. Moskvin, S. Grigoriev, P. Fouquet, and B. Farago, Phys. Rev. Lett. **102**, 197202 (2009).

[24] A. Bauer, M. Garst, and C. Pfleiderer, Phys. Rev. Lett. **110**, 177207 (2013).

[25] A. B. Butenko, A. A. Leonov, U. K. Rößler, and A. N. Bogdanov, Phys. Rev. B **82**, 052403 (2010).

[26] Y. Nishihara, S. Waki, and S. Ogawa, Phys. Rev. B **30**, 32 (1984).

[27] J. Teyssier, E. Giannini, V. Guritanu, R. Viennois, D. van der Marel, A. Amato, and S. N. Gvasaliya, Phys. Rev. B **82**, 064417 (2010).